NASA Contractor Report 198445
ICOMP–96–03; CMOTT–96–02

Calculations of Oblique Shock Wave/Turbulent Boundary-Layer Interactions With New Two-Equation Turbulence Models

William W. Liou
Institute for Computational Mechanics in Propulsion and
Center for Modeling of Turbulence and Transition
Cleveland, Ohio

P.G. Huang
MCAT, Inc.
Mountain View, California

January 1996

Prepared for
Lewis Research Center
Under Cooperative Agreement NCC3–370

National Aeronautics and
Space Administration

CALCULATIONS OF OBLIQUE SHOCK WAVE/TURBULENT BOUNDARY-LAYER INTERACTIONS WITH NEW TWO-EQUATION TURBULENCE MODELS

William W. Liou
Institute for Computational Mechanics in Propulsion and
Center for Modeling of Turbulence and Transition
NASA Lewis Research Center, Cleveland, Ohio

P.G. Huang
MCAT Inc.
Mountain View, California

ABSTRACT

Supersonic flows involving oblique shock wave/turbulent boundary-layer interactions are studied using the Favre-averaged Navier–Stokes equations and two recently developed $k-\varepsilon$, two–equation, eddy–viscosity models. The primary difference between these models and the existing $k-\varepsilon$ model is that the new models satisfy the realizability constraints of the Reynolds stresses. Three cases with different levels of shock strength were calculated. The corresponding flows were observed to be attached, near incipient separation, and with large separation zone, respectively. The computed results are compared with surface measurements for all the cases and, for the last case, where there is a large region of flow separation, measured mean and turbulent kinetic energy profiles are also available for comparison. The results show reasonable agreement with the measurements.

1. Introduction

With the advances of computational fluid dynamics, the design cycle for supersonic engine inlets can be greatly reduced through the use of Navier-Stokes solvers. A designer can essentially visualize the entire complex flow field projected by the solution of the Navier–Stokes equations, including features such as the interaction between the shock wave systems and the turbulent boundary layers, estimates the energy loss due to different agencies, and make necessary modifications prior to entering the wind tunnel. Therefore, an acceptable prediction capability for flows involving shock wave/turbulent boundary-layer interactions will not only enhance the performance of engine inlets, but also may deliver a significant reduction of its design cost. The present paper represents an attempt to address one of the pacing items to successfully predict flows of such nature, namely, the assessment of turbulence models. The aim is to evaluate two recently developed turbulent models in the calculations of the reflection of an oblique shock wave off a turbulent boundary layer, shown in Fig.1. Care has been taken to obtain solutions with a sufficiently refined computational grid and uniform initial and boundary conditions such that any differences observed in the results can be attributed to the turbulence models used in the calculations.

The incident shock is generated by a shock generator, normally a sharp-edged flat–plate inclined at an angle to the incoming supersonic stream. The incoming flow undergoes a deflection through the incident shock wave and another deflection through the reflected shock wave to become parallel to the bottom wall. The pressure rise, produced by the shock wave, propagates upstream in the subsonic portion of the boundary layer, causing the subsonic portion of the boundary layer to thicken. If the incident shock is sufficiently strong, the pressure rise may cause the boundary layer to separate, followed by the formation of a flow separation zone. The flow model, although geometrically simple, contains some important phenomena of the inlet flow field and is ideal for the assessment of the performance of turbulence models in such flows. The shock wave/turbulent boundary–layer interaction phenomenon is also of great practical interest for many industrial applications.

In the experimental flows considered here, the incoming flow conditions remain the same for all cases, with $M = 2.89$ and $Re = 5.73 \times 10^7/m$. The thickness of the test boundary layer is 1.694 cm. The shock strength is changed by varying the angle ($\theta = 7°, 10°,$ and $13°$) of the shock generator. While surface pressure and skin friction measurements were reported for all three angles, the mean velocity and turbulent kinetic energy profiles were available only for the 13° case, where a region of flow separation was observed. The flow fields produced by the particular model were studied extensively (Reda and Murthy, 1973a,b; Murthy and Rose, 1977; Modarress and Johnson, 1976). These studies include a rather detailed comparison of the mean velocity profiles measured using pressure probes and laser velocimetry (Modarress and Johnson, 1976) for the 13° case and quantitative comparisons of departures from two-dimensionality (Reda and Murthy, 1973a,b). Reda and Murphy (1973a) have reported that the surface oil flow

photographs showed more extensive departure from two-dimensionality for the 13° case than for the 7° case. However, the wall pressure distribution for the 13° case is more uniform in the spanwise direction than that for the 7° case.

Computationally, the flows have been studied using different numerical schemes and low-Reynolds number turbulence models at various levels (Viegas and Horstman, 1978; Haidinger and Friedrich, 1993). In general, the results showed no apparent superiority of a single model over the others. In this paper, two recently developed two-equation eddy-viscosity models are evaluated against these flows. The first model is a low-Reynolds number model and the second a high-Reynolds number model. A major improvement of the two new models is that the eddy-viscosity formulation includes explicitly the effect of the mean strain rate through the realizability constrains. The model, therefore, can be more suitable for flows where there are large or rapid changes of the mean flow. Flows involving interactions of oblique shock waves and turbulent bundary layers are, therefore, ideal test cases.

In the following sections, the turbulence models and the numerical platform used in this study are described. The results of flow calculations are then compared with those obtained by using two existing two-equation models, e.g., Chien's (1982) model (CH) and the standard $k-\varepsilon$ model (SKE).

II. ANALYSIS

Mean Flow Equations

The flow properties are decomposed into two parts: a mean value and a fluctuation with respect to the mean value. That is,

$$\hat{\rho} = \rho + \rho'' \tag{1.a}$$

$$\hat{u}_i = U_i + u_i' \tag{1.b}$$

$$\hat{p} = p + p'' \tag{1.c}$$

$$\hat{T} = T + T' \tag{1.d}$$

$$\hat{E} = E + E' \tag{1.e}$$

where ρ, p, T, E, U_i denote Reynolds-averaged density and pressure, mass-weighted-averaged temperature, total energy, and velocity, respectively. It is customary to use both the Reynolds average and the mass-weighted average in the decomposition process for compressible turbulent flows to simplify the final form of the mean flow equations. The governing equations for the mean flow may be obtained by substitution of flow properties in the form (1) into the Navier-Stokes equations followed by a Reynolds average of the equations. The mean flow equations become,

$$\rho_{,t} + (\rho U_i)_{,i} = 0 \tag{2.a}$$

$$(\rho U_i)_{,t} + (\rho U_i U_j + \tau_{ij} + p\delta_{ij})_{,j} = 0 \tag{2.b}$$

$$(\rho E)_{,t} + (\rho U_i E + pU_i + q_{T,i} + \tau_{ij}U_j + q_{k,i})_{,i} = 0 \tag{2.c}$$

where

$$\tau_{ij} = 2(\mu + \mu_t)S_{ij} - \frac{2}{3}k\delta_{ij}$$

μ denotes the mean molecular viscosity and S_{ij} denotes the mean strain rate tensor, i.e.,

$$S_{ij} = \frac{1}{2}(U_{i,j} + U_{j,i}) - \frac{1}{3}U_{k,k}\delta_{ij} \tag{3}$$

The turbulent Reynolds stresses are modeled via the turbulent eddy viscosity, μ_t. In all of the models used in this study, the turbulent eddy viscosity is determined by the turbulent kinetic energy, k, and the dissipation rate, ε, i.e.,

$$\mu_t = C_\mu f_\mu \rho \frac{k^2}{\varepsilon} \tag{4}$$

k and ε are obtained from the solution of their respective model transport equations. f_μ is the wall damping function for the eddy-viscosity. For reference, these models are described briefly in the following.

Turbulence Models

In Shih et. al (1994), a general constitutive relation between the Reynolds stresses and the mean flow deformation rate was derived by using the invariance principle of Lumley. The model satisfies the realizability constraints: for example, the energy component $\overline{u_1 u_1}$ should always be positive. Note that the standard $k-\varepsilon$ model with $C_\mu = 0.09$ is an unrealizable model. For example, $\overline{u_1 u_1}$ becomes negative when

$$\frac{S_{11}k}{\varepsilon} > \frac{1}{0.27}. \tag{5}$$

Therefore, the value of C_μ should not be a constant for a realizable model. In Shih et. al (1994), the realizability constraints have led to,

$$C_\mu = \frac{1}{A_0 + A_s U^{(*)}\frac{k}{\varepsilon}} \tag{6}$$

where

$$U^{(*)} = \sqrt{S_{ij}S_{ij} + \tilde{\Omega}_{ij}\tilde{\Omega}_{ij}}$$

$$\tilde{\Omega}_{ij} = \tilde{\Omega}_{ij} - 2\epsilon_{ijk}\omega_k$$

$$\tilde{\Omega}_{ij} = \Omega_{ij} - \epsilon_{ijk}\omega_k$$

Ω_{ij} is the mean rotation rate viewed in a rotating reference frame with the angular velocity ω_k. The parameter A_s is determined by

$$A_s = \sqrt{6}\cos\phi, \quad \phi = \frac{1}{3}arc\cos(\sqrt{6}W)$$
$$W = \frac{S_{ij}S_{jk}S_{ki}}{\tilde{S}^3} \quad \tilde{S} = \sqrt{S_{ij}S_{ij}} \tag{7}$$

The new formulation of C_μ, with an explicit dependence on the mean strain rate, can be used to render a model realizable. It is also in accord with experimental observations

that the value of C_μ can be different for different flows. The value of A_0 is set equal to 4.0 (Shih et. al, 1995). It is determined by examining the log–law of the inertial sublayer. The corresponding value of C_μ is 0.09. As was noted by Shih et. al (1995), the resulting formulation for C_μ also worked very well for homogeneous shear flows. The first model tested here was the Shih and Lumley (1993) model, modified by including the new formulation of C_μ (Yang et. al 1995). The second model by Shih et. al (1995), on the other hand, has applied the variable C_μ formulation during the development of the model.

• Shih and Lumley (1993) — KE1

The model equations for k and ε in KE1 model are,

$$\rho k_{,t} + \rho U_i k_{,i} = [(\mu + \mu_t)k_{,i}]_{,i} - \rho\widetilde{u_i u_j}U_{i,j} - \rho\varepsilon \quad (8.a)$$

$$\rho\varepsilon_{,t} + \rho U_i\varepsilon_{,i} = [(\mu + \frac{\mu_t}{\sigma_\varepsilon})\varepsilon_{,i}]_{,i} - C_1\frac{\varepsilon}{k}\rho\widetilde{u_i u_j}U_{i,j} - C_2 f_2\rho\frac{\varepsilon^2}{k} + \nu\mu_t U_{i,jk}U_{i,jk} \quad (8.b)$$

where

$$C_1 = 1.44, \quad C_2 = 1.92, \quad \sigma_\varepsilon = 1.3$$

$$f_2 = 1 - 0.22\exp[-(\frac{R_t}{6})^2], \quad R_t = \frac{k^2}{\nu\varepsilon}$$

The damping function is defined by

$$f_\mu = [1. - \exp(-(a_1 R_k + a_3 R_k + a_5 R_k))]^{\frac{1}{2}} \quad (9)$$

where

$$a_1 = 1.7 \times 10^{-3}, \quad a_3 = 10^{-9}, \quad a_5 = 5 \times 10^{-10}$$

$$R_k = \frac{\rho\sqrt{k}y}{\mu}$$

Note that the value a_1 has been modified due to the application of the new formulation of variable C_μ which is bounded by 0.09 in the current application. This modified Shih and Lumley (1993) model has been shown to predict well a variaty of flows in Yang et al. (1995). The near–wall boundary conditions for the turbulent quantities are determined by examining the Kolmogorov behavior of near-wall turbulence proposed by Shih and Lumley (1993). They have shown that energetic eddies reduce to "Kolmogorov eddies" at a finite distance from the wall and all the wall parameters are characterized by Kolmogorov microscales. Therefore, an estimate can be obtained for the turbulent kinetic energy and its dissipation rate at the location where large eddies become Kolmogorov eddies by using both direct numerical simulation results and an asymptotic analysis of near wall turbulence. According to their analysis, this turbulent limit point is located at

$$y_\eta = \frac{6\nu}{u_\tau} \quad (10)$$

At this limit point,

$$k_\eta = 0.25u_\tau^2 \quad \text{and} \quad \varepsilon_\eta = 0.251\frac{u_\tau^4}{\nu} \quad (11)$$

With the application of eqns.(10) and (11), the turbulent time scale near a wall, similar to the velocity and length scales, is determined by the Kolmogorov time scale. Therefore, there is no unphysical singularity in the current model ε equation.

• Shih et. al (1995) — KE2

A new form of model equation for the turbulent dissipation rate was proposed by Shih et. al (1995). The equation for the mean-square vorticity fluctuation was first examined by using an order of magnitude analysis. The truncated low-order equation is then modeled through physical reasonings. The modeled equation for the mean-square vorticity fluctuation can be transformed into an equation for the turbulent dissipation rate in the limit of high Reynolds number. The resulting model equation for ε is,

$$\rho\varepsilon_{,t} + \rho U_j\varepsilon_{,j} = [(\mu + \frac{\mu_t}{\sigma_\varepsilon})\varepsilon_{,j}]_{,j} + C_1\rho S\,\varepsilon - C_2\rho\frac{\varepsilon^2}{k + \sqrt{\nu\varepsilon}} \quad (12)$$

where

$$C_1 = max\{0.43, \quad \frac{\eta}{5+\eta}\}, \quad \sigma_\varepsilon = 1.2, \quad C_2 = 1.9$$

$$S = \sqrt{2S_{ij}S_{ij}}, \quad \eta = \frac{Sk}{\varepsilon}$$

In Shih et. al (1995), the new modeled dissipation rate equation was coupled with the standard model equations for k, eq.(8.a), to form a two–equation model. Because $\sqrt{\nu\varepsilon}$ appears in the denominator of the sink term, this new dissipation rate equation will not become singular even if k vanishes. C_μ is defined by eq.(6). Near the wall, a compressible wall-function was applied.

$$\frac{u_c}{u_\tau} = \frac{1}{\kappa}ln(y^+) + C \quad (13)$$

u_c is the Van Driest transformed velocity defined as,

$$u_c = \sqrt{B}[arcsin(\frac{A+U}{D}) - arcsin(\frac{A}{D})] \quad (14)$$

where

$$A = \frac{q_w}{\tau_w}, \quad B = \frac{2c_p T_w}{Pr_t}, \quad D = \sqrt{A^2 + B}$$

The heat flux near the wall is defined as,

$$q = q_w + U\tau \quad (15)$$

The turbulent quantities are defined as,

$$k = \frac{\tau_w/\rho}{\sqrt{C_\mu}}, \quad \varepsilon = \frac{(\tau_w/\rho)^{3/2}}{\kappa y} \tag{16}$$

The value of y^+ for the first grid point away from the wall, where the wall-function is applied, is around 30. Although the validity of the wall–function in complex separated flows is somewhat ambiguous, previous work seems to show that it can provide reasonably accurate prediction for a wide range of flows (Huang and Coakley, 1993a; Huang and Liou, 1994).

It should be noted that except for the mean flow volume dilatation, no explicit compressibility effect models have been included in any of the models in the calculations performed in this study.

The results of calculations using these two realizable models, which are presented in a later section, are compared with those obtained by using the standard $k-\varepsilon$ model (SKE) and Chien's (1982)(CH) low–Reynolds number $k-\varepsilon$ model. The SKE and CH models are representative in the high– and low–Reynolds number classes of models, respectively. They are chosen here for comparison due to their simplicity and stability. In the following, the numerical solution procedure is described.

Numerical Solutions

The Favre–averaged Navier-Stokes equations and the model transport equations were solved numerically by using the COMTUR code developed by Huang and Coakley (1992). Briefly, it uses a line-by-line Gauss-Seidel algorithm and Roe's approximate Riemann solver. Yee's MINMOD TVD scheme was applied in all the computations. The mean and the turbulence equations are solved in a sequential manner. All the calculations were carried out with the same initial and boundary conditions, including those for k and ε. At the inlet of the computational domain, a fully developed flat–plate turbulent boundary layer with the measured displacement thickness (δ^*=0.388cm) was prescribed using the SKE and CH model solution of the flow for the high– and low–Reynolds number models, respectively. Grid-refinement studies were performed for the least forgiving 13° case, where the boundary layer separates, with 110×60, 120×80, 120×100, and 160×80 grid nodes. KE2 model was used in these calculations. It was found that a grid-independent solution could be obtained with the 120×80 grid. There are, typically, about forty to fifty grid points inside the boundary layer. Similarly, for the low–Reynolds number models, a 130×100 grid was found sufficient. The same grids were then used for all the cases of different shock strengths and turbulence models.

III. RESULTS AND DISCUSSIONS

The experimental flows studied involve the interaction of oblique shock waves and a turbulent boundary layer in a two-dimensional channel at an incoming flow Mach number of 2.87. At a shock generator angle of $\theta = 7°$, the interaction is rather weak and the turbulent boundary layer remains attached. Fig.2a shows the computed and the measured variations of the wall pressure (normalized by the stagnation pressure of the incoming stream). Streamwise distance, x, is measured relative to the projected inviscid shock impingment point. The boundary–layer thickness of the incoming stream is denoted by δ_0. The results obtained by using the four models are essentially the same, which predict well the overall pressure rise. However, the model predictions reach the pressure plateau earlier than the measurement. It indicates that the models have predicted a relatively faster relaxation from the effect of the shock waves than is observed in the experiment.

Fig.2b shows the comparison of the calculated and the measured skin friction coefficients. The observed decrease of the skin friction upstream of the projected inviscid shock impingement point is not predicted well by any of the four models. Near the shock impingement point, CH model predicts a relatively fast development of the boundar layer compared with those predicted by the other three models. In the recovery region, the measurement shows that the boundary layer relaxes toward a higher value of the skin friction coefficient than the predictions. This, however, should not be regarded as a model deficiency since the skin friction coefficient for flat–plate turbulent boundary layers predicted by all the three models tested here agrees well with the Van Driest II formula, which represents a curve fit of many flat–plate boundary–layer skin friction measurements.

The predictions and the measurement of the surface parameters for $\theta = 10°$ are shown in Fig.3. The model predictions of the location where an abrupt change of the skin friction coefficient occures, indicating a flow deceleration due to, in this case, the adverse pressure gradient, are roughly the same. The meassured skin friction shows that the flow is near incipient separation. The flow predicted by KE2 model is the nearest to incipient separation. It is followed by SKE, KE1, and CH models. CH model shows a rather distinct pattern of skin friction variation compared with the other models. It is well known that CH model returns abnormally high length scale, $k^{3/2}/\varepsilon$, near the viscous sublayer when subjected to adverse pressure gradient. The resulting increase in eddy–viscosity can thus lead to a corresponding rise in skin friction coefficient. There are measures to correct this model defect. For instance, Huang and Coakley (1993b) proposed to use the von Kármán length scale to limit the calculated length scale. In the current calculations, no corrections of any kind were used. Despite the difference in the skin friction variation, the wall pressure predictions, shown in Fig.3b, are essentially the same for all the models. It shows that the aberrant estimate of the length scale in CH model occures locally and has not affected the development of the flow far away from the wall.

The streamwise distributions of the skin friction coefficient and the wall pressure for $\theta = 13°$ are compared in Fig.4. In this case, the shock strength is sufficiently strong to cause large flow separation. As inferred from the skin friction coefficient results, this region of flow separation is

predicted by all the four models. Compared with CH and SKE models, KE1 and KE2 models give slightly better prediction for the streamwise location where the drop in the value of skin friction first occurs. The predicted streamwise extent of the separation zone obtained by using the four different models are largely the same, which appears to be smaller than the measurement. The models, however, do not share the similarity in their responses to the strong interactions between the shock wave and the boundary layer. The high–Reynolds number models, e.g. SKE and KE2 models, give better predictions for the overall variation of the skin friction coefficient than the low–Reynolds number CH and KE1 models. It should be noted that the wall–function used in the calculations with high–Reynolds number models, e.g. KE2 and SKE models, does not include the effect of pressure gradient. It is likely that the high–Reynolds number model results can be improved if the pressure gradient effects are explicitly included in the wall–function boundary conditions. Between the two low–Reynolds number models, KE1 model give much better relaxation of the skin friction after the flow reattaches than CH model. All the four models, however, return higher rate of flow recovery than indicated by the measurement.

KE1 and KE2 models give a better prediction of the upstream interaction length, indicated by the earlier rise of the predicted wall pressure. Overall, KE1 and KE2 models give a streamwise variation of the wall pressure similar to that produced by SKE model. The wall pressure prediction given by CH model is less desireable in this strong interaction case. For instance, at $x = 0$, SKE, KE1, and KE2 models overpredicted the wall pressure by about 7%. For CH model, the overprediction is nearly 20%. Note that the wall pressure predictions are essentially the same when the boundary layer reamins attached, i.e., for $\theta = 7^0$ and 10^0. The poor performance of CH model in predicting surface parameters when the boundary layer separates is believed to be due to the abnormally large predicted length scale near the viscous layer.

Measured and predicted mean streamwise velocity profiles for $\theta = 13°$ are shown in Fig.5. At x/δ_0=–4.21, the model predictions are essentially the same. Since all the four models used here have been shown to predict very well the flat–plate turbulent boundary layer, this similarity is not unexpected. In the region of strong interactions, say, from x/δ_0=–2.7 to 0.29, the trend of variation of the mean velocity is basically captured by all the models, with the KE1 model showing the greatest sensitivity to the effect of the shocks. The predicted locations of reflected shock are also nearly the same for all the models. Downstream of the flow reattachment, say, x/δ_0= 0.29 and 2.54, KE1 model give good representation for the mean velocity. The flow predicted by CH model seems to recover at a higher pace than the other models, which conforms with the previous observations.

Comparisons of the model prediction of the turbulent kinetic energy and experimental data are shown in Fig.6. In the region of strong interactions, the predicted location of the maximum turbulent kinetic energy moves upward toward the shear layer where large turbulent production occurs. All four models, however, underpredict the kinetic energy level in the recirculation zone by about a factor of two to three. This indicates that the models did not capture the strong non-equilibrium resulting from the interaction process. The apparent agreement of the turbulent kinetic energy profiles between the measurement and the model predictions downstream of the flow reattachment, therefore, may be a result of a slower relaxation of turbulent structures returned by the models. The high turbulent intensity returned by CH model downstream of the flow reattachment has resulted in the fast development of the mean flow, Fig.5.

In Fig.7, the values of the coefficient for the turbulent eddy viscosity, C_μ, are compared. Note that for SKE and CH models, the value of C_μ is a constant of 0.09. For KE1 and KE2 models, the value of C_μ varies with the local mean strain rate. At x/δ_0=–4.21, the values returned by KE1 and KE2 models are roughly 0.09 across the boundary layer, again, suggesting that the turbulent boundary layer is hardly disturbed by the interactions. At x/δ_0=–2.7, where the effect of the interactions are strong, the distributions for KE1 and KE2 model bear little resemblence. Further downstream, as the flow develops, they gradually become similar. Note that, for KE2 model, the maximum value for C_μ which occurs when either the mean stain rate or the turbulent kinetic energy vanishes is about 0.25. For KE1 model, the value of C_μ is bounded by 0.09. In the near wall region, the value of C_μ for KE2 model increases rapidly as the flow develops. This may have resulted in the higher values of the skin friction behind the inviscid shock impingement point for KE2 model.

IV. SUMMARY

Predictions of shock wave/turbulent boundary–layer interactions using the modified Shih and Lumley (1993) and the Shih et. al (1995) models are reported in this paper. Comparisons with the standard $k - \varepsilon$ model and the Chien(1982) model has also been presented. For calculations with the same type of model, i.e., high– vs. low–Reynolds number models, the same inlet conditions and grids were used.

All the four models predict reasonably well the mean velocity distribution. For high–Reynolds number models, the Shih et. al (1995) model performs similarly to the standard $k - \varepsilon$ model in both weak and strong interaction cases. The low–Reynolds number model of Shih et. al (1995a) give significantly better solution than Chien's (1982) model, particularly in the case with strong interactions. The results show that the modified Shih and Lumley (1993) model is more responsive in situations where the mean flow changes rapidly. In the case of the strong interaction, the upstream interaction length predicted by the two new models agree better with the measurement than the two existing models tested.

REFERENCES

Chien, K.-Y., 1982, "Predictions of Channel and Boundary–Layer Flows with a Low Reynolds Number Turbulence Model," *AIAA Journal*, Vol. 20, pp.33-38.

Haidinger, F. A. and Friedrich, R., 1993, "Computation of Shock Wave/Turbulent Boundary Layer Interactions Using a Reynolds Stress Model," Ninth Symposium on Turbulent Shear Flows.

Huang, P. G. and Coakley, T. J., 1992, "An Implicit Navier-Stokes Code for Turbulent Flow Modeling," AIAA paper 92-0547.

Huang, P. G. and Coakley, T. J., 1993a, "Calculations of Supersonic and Hypersonic Flows Using Compressible Wall Functions," Second International Symposium on Engineering Turbulence Modeling and Measurement, Florence, Italy.

Huang, P. G. and Coakley, T. J., 1993b, "Turbulence Modeling for Complex Hypersonic Flows," AIAA paper 93-0200.

Huang, P. G. and Liou, W. W., 1994, "Numerical Calculations of Shock–Wave/Boundary–Layer Flow Interactions," NASA TM 106694.

Modarress, D. and Johnson, D.A., 1976, "Investigation of Shock-Induced Separation of a Turbulent Boundary Layer Using Lazer Velocimetry," AIAA paper 76-374.

Murthy, V. S. and Rose, W. C., 1977, "Direct Measurements of Wall Shear Stress by Buried Wire Gages in a Shock Wave - Boundary Layer Interaction Region," AIAA paper 77-691.

Reda, D. C. and Murthy, J. D., 1973a, "Shock Wave/Turbulent Boundary-Layer Interaction in Rectangular Channels," *AIAA Journal*, Vol. 11, pp. 139-140.

Reda, D. C. and Murphy, J. D., 1973b, "Sidewall Boundary-Layer Influence on Shock Wave/Turbulent Boundary-Layer Interactions," *AIAA Journal*, Vol.11, pp.1367-1368.

Shih, T. H. and Lumley, J. L., 1993, "Kolmogorov Behavior of Near–Wall Turbulence and Its Application in Turbulence Modeling," *Comp. Fluid Dyn.*, Vol. 1, pp.43-56.

Shih, T. H., Zhu, J., and Lumley, J. L., 1994, "A New Reynolds Stress Algebraic Equation Model," NASA TM 106644. Accepted for publication in *Comput. Methods Appl. Mech. Eng.*.

Shih, T. H., Liou, W. W., Shabbir, A., Yang, Z., and Zhu, J., 1995, "A New $k-\varepsilon$ Eddy Viscosity Model for High Reynolds Number Turbulent Flows," *Computers Fluids*, Vol. 24, pp.227-238.

Viegas, J. R. and Horstman, C. C., 1978, "Comparison of Multiequation Turbulence Models for Several Shock Separated Boundary-Layer Interaction Flows," AIAA paper 78-1165.

Yang, Z., Georgiadis, N., Zhu, J., and Shih, T.-H., "Calculations of Inlet/Nozzle Flows Using a New $k-\varepsilon$ Model," AIAA paper 95-2761.

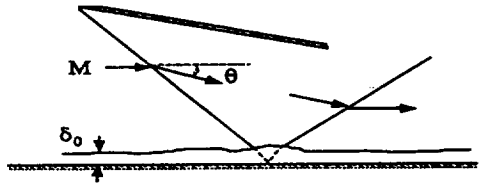

Figure 1. Sketch of oblique shock/boundary–layer interaction.

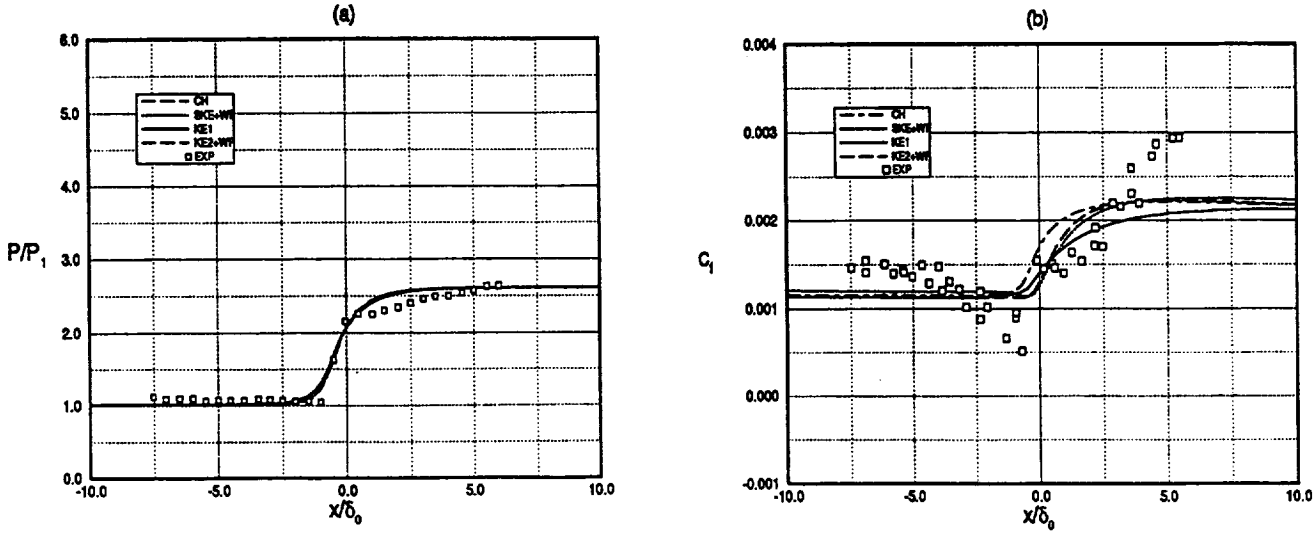

Figure 2. Comparison of wall surface parameters. $\theta = 7°$. (a) Normalized Pressure; (b) Skin friction coefficient.

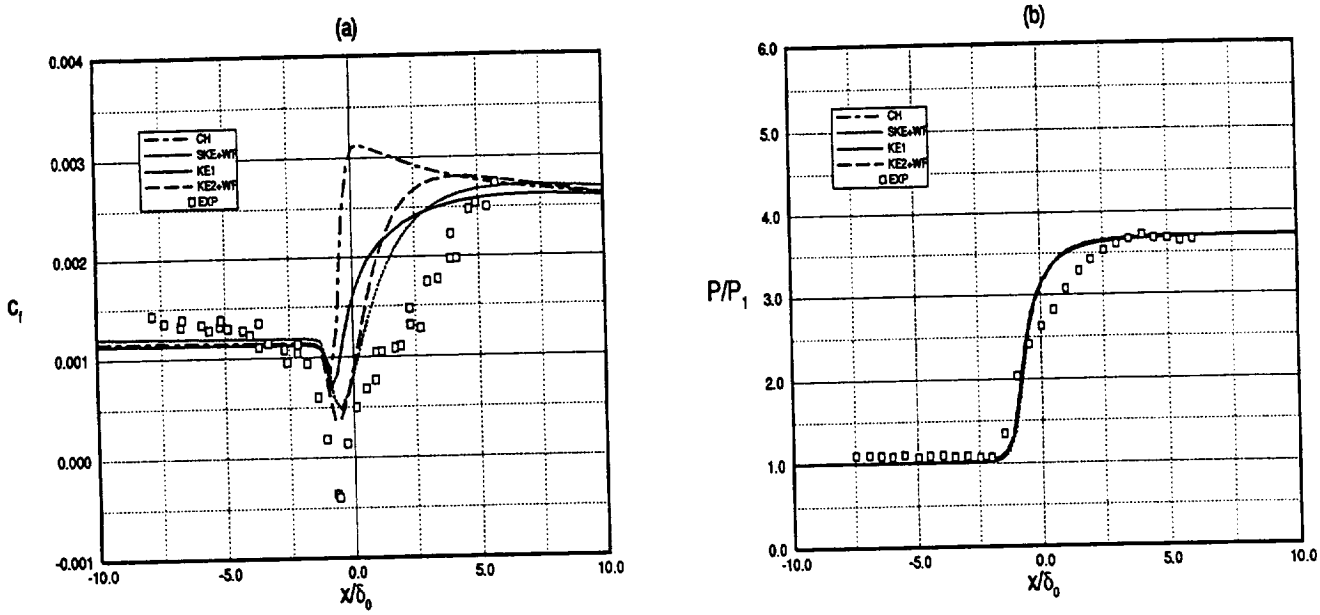

Figure 3. Comparison of wall surface parameters. $\theta = 10°$. (a) Skin friction coefficient; (b) Normalized Pressure.

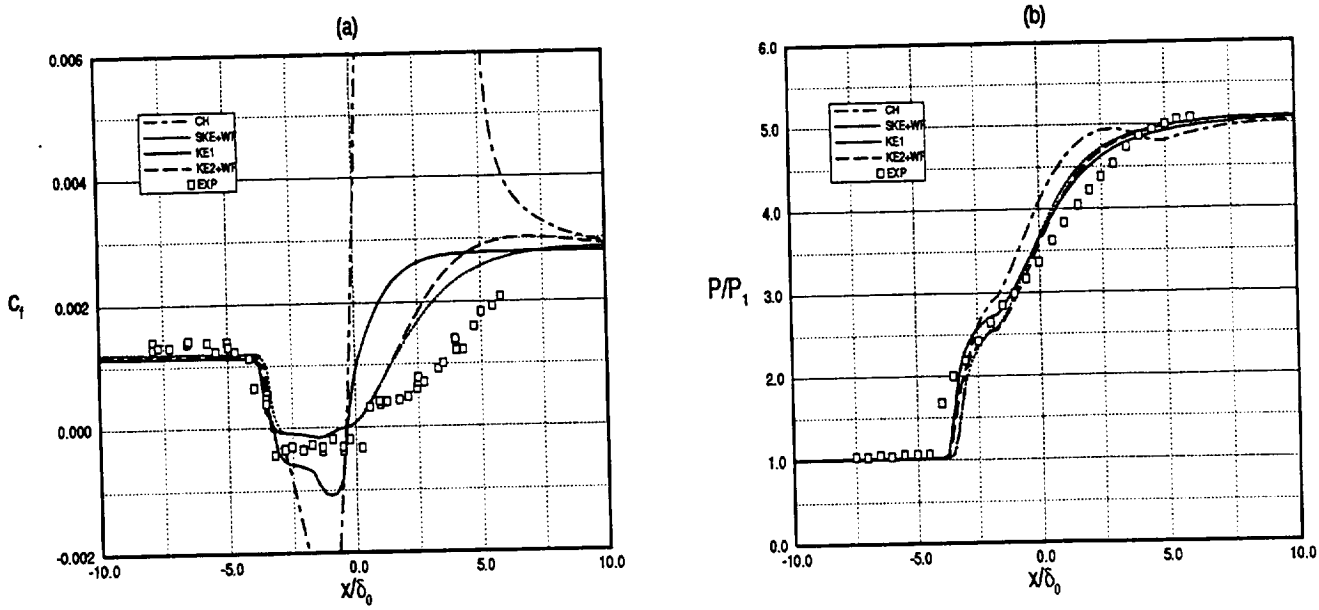

Figure 4. Comparison of wall surface parameters. $\theta = 13°$. (a) Skin friction coefficient; (b) Normalized Pressure.

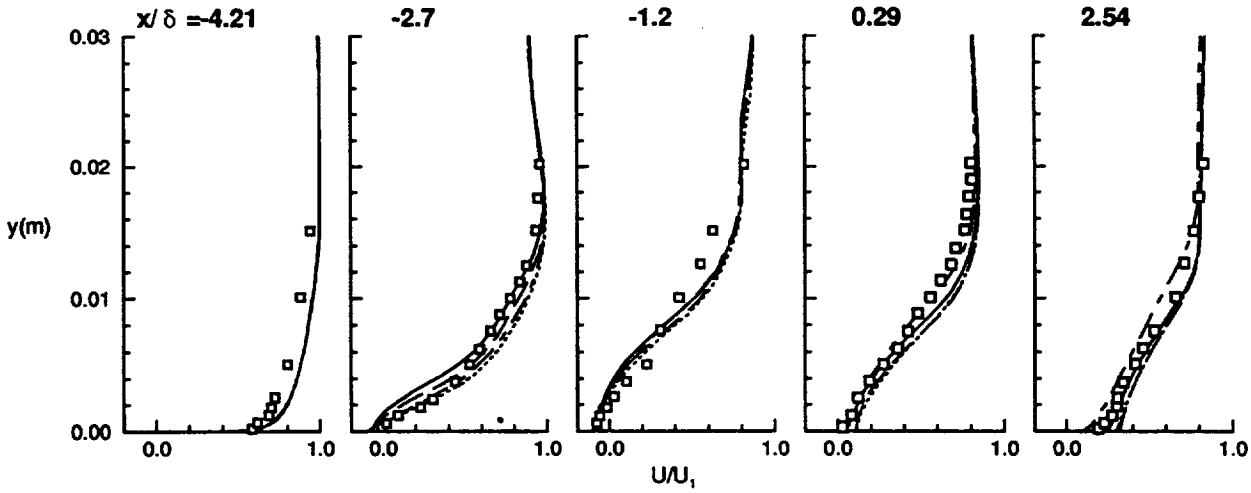

Figure 5. Comparison of mean streamwise velocity profile. $\theta = 13°$. — - —, CH model; - - - - -, SKE model; ——, KE1 model; – – –, KE2 model; □, measurement.

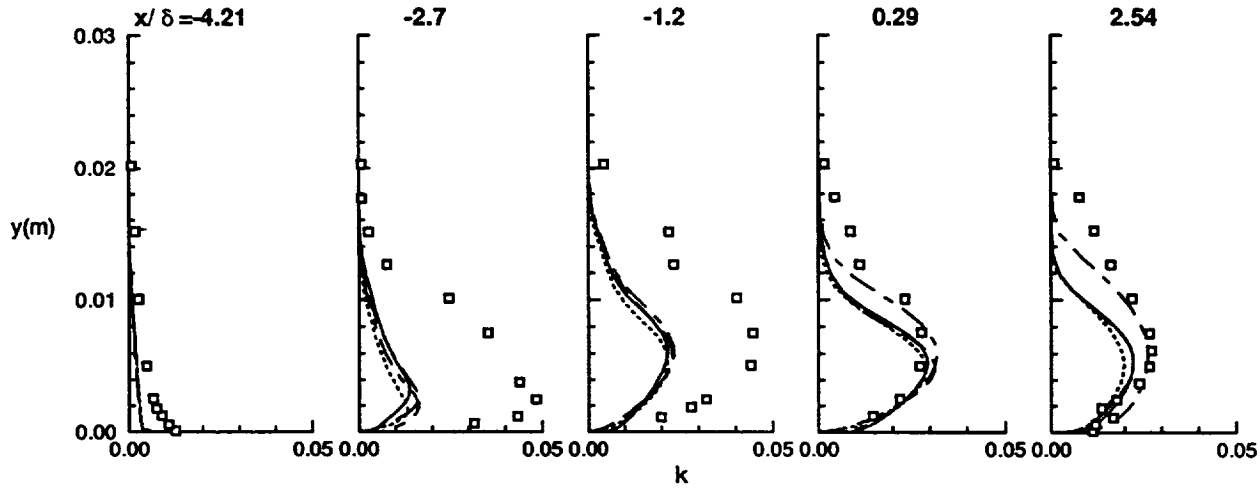

Figure 6. Comparison of turbulent kinetic energy profile. $\theta = 13°$. Legend: see Figure 5.

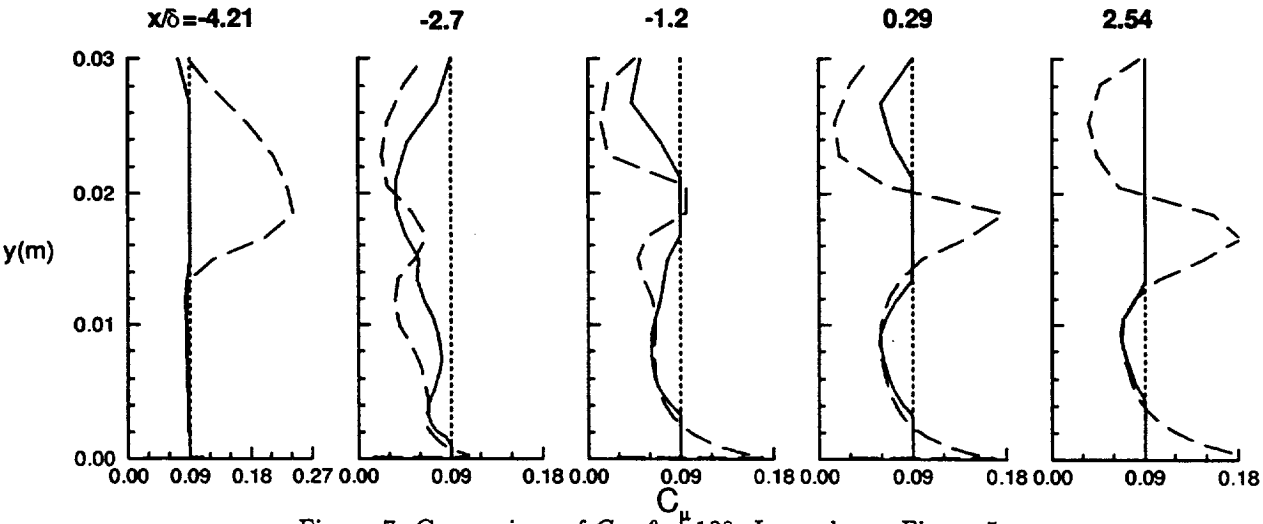

Figure 7. Comparison of C_μ. $\theta = 13°$. Legend: see Figure 5.

REPORT DOCUMENTATION PAGE

Form Approved
OMB No. 0704-0188

1. AGENCY USE ONLY (*Leave blank*)	2. REPORT DATE	3. REPORT TYPE AND DATES COVERED
	January 1996	Contractor Report

4. TITLE AND SUBTITLE

Calculations of Oblique Shock Wave/Turbulent Boundary-Layer Interactions With New Two-Equation Turbulence Models

5. FUNDING NUMBERS

WU–505–90–5K
NCC3–370

6. AUTHOR(S)

William W. Liou and P.G. Huang

7. PERFORMING ORGANIZATION NAME(S) AND ADDRESS(ES)

Institute for Computational Mechanics in Propulsion
22800 Cedar Point Road
Cleveland, Ohio 44142

8. PERFORMING ORGANIZATION REPORT NUMBER

E–10084

9. SPONSORING/MONITORING AGENCY NAME(S) AND ADDRESS(ES)

National Aeronautics and Space Administration
Lewis Research Center
Cleveland, Ohio 44135–3191

10. SPONSORING/MONITORING AGENCY REPORT NUMBER

NASA CR–198445
ICOMP–96–03
CMOTT–96–02

11. SUPPLEMENTARY NOTES

Prepared for the Joint Fluids Engineering Conference cosponsored by the ASME, JSME, and European Association for Laser Anemometry, Hilton Head Island, South Carolina, August 13–18, 1995. William W. Liou, Institute for Computational Mechanics in Propulsion and Center for Modeling of Turbulence and Transition, NASA Lewis Research Center (work funded by NASA Cooperative Agreement NCC3–370); P.G. Huang, MCAT, Inc., Mountain View, California. ICOMP Program Director, Louis A. Povinelli, organization code 2600, (216) 433–5818.

12a. DISTRIBUTION/AVAILABILITY STATEMENT

Unclassified - Unlimited
Subject Category 34

This publication is available from the NASA Center for Aerospace Information, (301) 621–0390.

12b. DISTRIBUTION CODE

13. ABSTRACT (*Maximum 200 words*)

Supersonic flows involving oblique shock wave/turbulent boundary-layer interactions are studied using the Favre-averaged Navier-Stokes equations and two recently developed $k-\varepsilon$, two-equation, eddy-viscosity models. The primary difference between these models and the existing $k-\varepsilon$ model is that the new models satisfy the realizability constraints of the Reynolds stresses. Three cases with different levels of shock strength were calculated. The corresponding flows were observed to be attached, near incipient separation, and with large separation zone, respectively. The computed results are compared with surface measurements for all the cases and, for the last case, where there is a large region of flow separation, measured mean and turbulent kinetic energy profiles are also available for comparison. The results show reasonable agreement with the measurements.

14. SUBJECT TERMS

Turbulence modeling; Shock/boundary layer interaction

15. NUMBER OF PAGES

10

16. PRICE CODE

A02

17. SECURITY CLASSIFICATION OF REPORT	18. SECURITY CLASSIFICATION OF THIS PAGE	19. SECURITY CLASSIFICATION OF ABSTRACT	20. LIMITATION OF ABSTRACT
Unclassified	Unclassified	Unclassified	

National Aeronautics and
Space Administration

Lewis Research Center
Cleveland, OH 44135-3191